A NOVEL CHARGE-COUPLED DEVICE FOR TIME DELAY WITHIN-PULSE SECTOR SCANNING SONARS

L. H. Ong

Abstract: Computer simulation studies and experimental evaluation of existing Time-Delay-and-Integrate devices for within pulse sector scanning demonstrate the presence of beam distortions which depend on sector size, beamwidth and scanning rate. Severe distortions prevent the potential application of such devices to high speed scanning. A new device structure based on a novel concept of time delay beam scanning is reported, which is specially suited for fast scanning without distortions.

I. Introduction

In Time Delay and Integrate (TDI) signal processing, signals from parallel channels are differentially delayed before being summed or integrated into a serial output as shown in fig. 1.1a. The actual TDI device[1] used in this work is more accurately represented by a fig 1.1b where each input is added to the accummulating sum of preceding inputs obtained at different past instants in time depending on the clock history.

Fig 1.2 shows plane waves impinging on a line array of equally spaced transducers which are connected in order to the TDI. With the TDI operated at a constant clock period τ_p, constructive summation occurs for wavefronts coming from direction θ_p for which the delay in water equals the delay introduced by the device. The TDI therefore 'forms a beam' in a direction determined by the clock period.

There are basically three ways of using TDI devices to look at a sector.

In the pulse to pulse approach, after a pulse is transmitted, the TDI clock period is maintained constant for the time that the pulse takes to travel out to the maximum range and return. For each pulse, the clock period is constant at a different value to look at a different direction. Taking as an example, a maximum range of 75 metres and a sector containing 30 beams, the total sector coverage time is 3 seconds. This is evidently a slow beam steering application.

Secondly, multiple beams can be preformed by operating a number of TDI devices in parallel each at a different clock period to look at a different angle. Sector coverage is attained by either displaying the TDI outputs simultaneously or scanning them serially. This approach presents no new problems though the use of separate clock generator and peripheral circuitry for each device may lead to system complexity. Beam interpolation may be required.

This paper however is mainly concerned with evaluating the TDI for within pulse sector scanning in which the receive 'beam' is swept across the insonified sector within the duration of the transmitted pulse so that no target is lost. For good range resolutions, short pulses are used. Presently available sector scanning sonars using phase scanning have been operated at scanning rates of more than 5 kHz (pulse durations less than 200 microseconds). It is the aim of this work to evolve a time delay scanning system capable of the same fast scanning rates and with the attendant wide bandwidth advantages of time delay processing. The system simplicity and compactness accruing from the use of TDI devices are also important considerations.

Unlike the first two approaches where constant period clocks are used, the TDI is in this case driven with a scanning clock whose period varies from period to period within a scan. The next section is concerned with problems encountered with the existing TDI devices when the clock period is varied rapidly as is necessary at high scanning rates.

L. H. ONG is with the Department of Electronic and Electrical Engineering, University of Birmingham, U. K.

II. Beam Distortions at High Scanning Rates

Fig 2.1 shows the situation when the TDI is operated with a scanning clock where the successive clock periods are different as denoted by τ_1, τ_2, τ_3, etc. At the instant when the clock period τ_1 is equal to the delay in water τ_ω between adjacent transducers, the first two input samples A and B are constructively summed together since they are taken from the same plane wavefront. However, at the next sampling instant, the clock period τ_2 being different from τ_1, the third input sample does not come from the point C on the same wavefront but from a point either in front of or behind C, depending on whether τ_2 is smaller or larger than τ_1. In Fig 2.1, τ_2 is assumed larger than τ_1 and hence a point C' behind C is sampled. The time difference between C and C' therefore constitutes a scanning time error. These scanning time errors are cumulative and become progressively worse for subsequent inputs. The extent of these errors will of course depend on the way the successive clock periods are varying and thus on how the 'beam' is swept over the sector. It is desirable to sweep the 'beam' at a constant speed over the sector in order to ease the display and interpretation of bearing information on a linear angular scale. For a constant speed scan, the instantaneous scanning clock period must vary linearly with time as shown in fig 2.2. In Appendix I, it is shown that with such a linear period-modulated clock, the successive clock periods form a geometrical progression with a common ratio $\gamma = 1+r$, where r is the rate of change of clock period. The successive clock periods in Fig 2.1 are thus related $\tau_2 = \tau_1 \gamma$, $\tau_3 = \tau_1 \gamma^2$, $\tau_4 = \tau_1 \gamma^3$, etc.

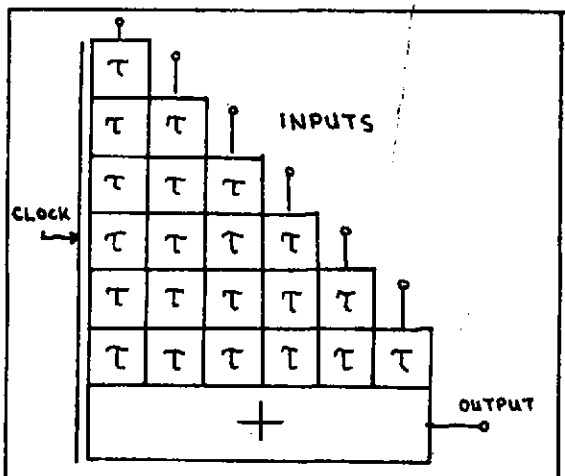

(a) Multiple delay lines

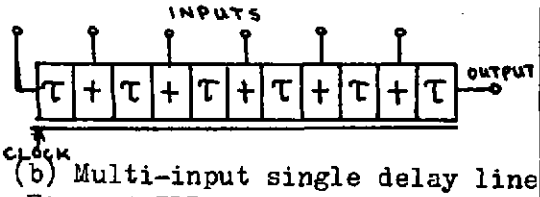

(b) Multi-input single delay line

Fig 1.1 TDI Representations

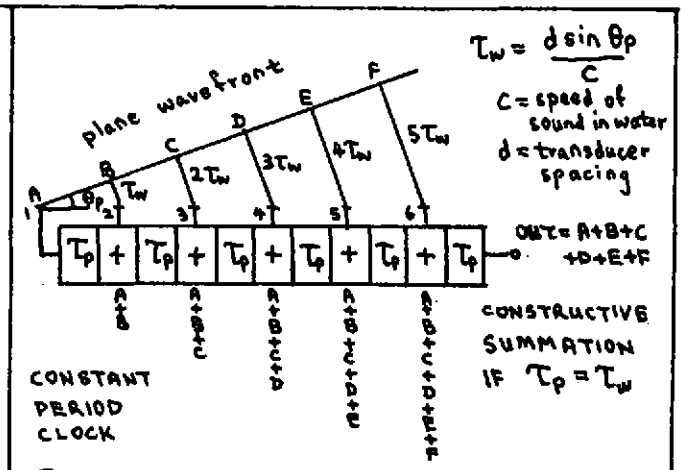

Fig 1.2 TDI beamforming

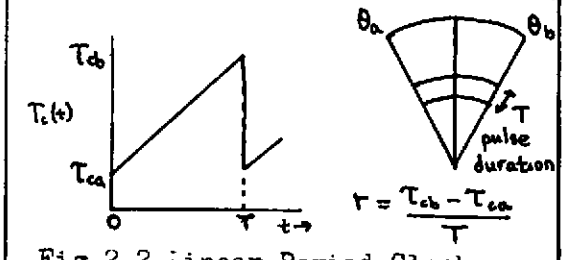

Fig 2.2 Linear Period Clock

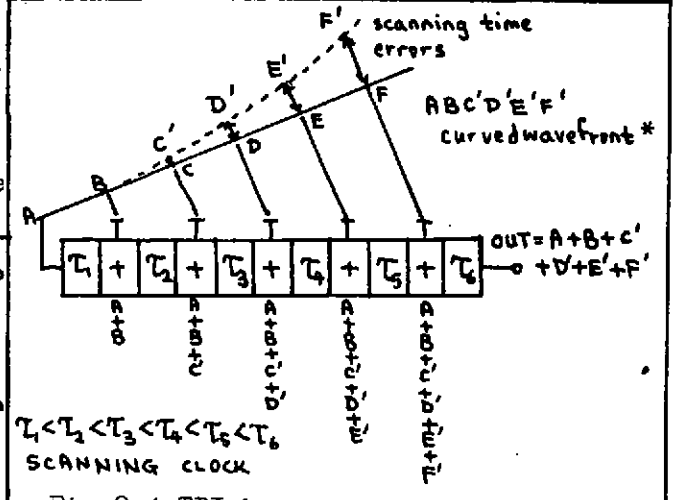

Fig 2.1 TDI beam scanning

*It is to be appreciated that the radius of curvature of the curved wavefront resulting from the scanning clock varies not only over the wavefront but also with the angle of incidence.

What are the factors that affect the scanning time errors? Firstly, if the scanning rate is increased, the clock period has to be swept at a faster rate and the successive clock periods are consequently much MORE different from one another. Hence, larger scanning errors ensue. Secondly, it can be seen from Fig 2.1 that a larger array aperture size results in not only more but also larger time errors. Thirdly, and of crucial significance, the scanning errors increase with the angle of incidence since the larger the successive clock periods, the more different they are from one another. A quantitative analytical expression for the n th input scanning time error can be derived in terms of these factors as follows:

$$S.T.E. = (n-1)\tau_w\gamma\left[1 - \tfrac{1}{\gamma} + \sum_{l=1}^{\infty}\left\{(-1)^l\, {}^{n+l-1}C_{n-1}\,\frac{\gamma^l}{(l+1)}\right\}\right]$$

where $ {}^{j}C_{k} = j!/(j-k)!k!$

However, a more informative way of monitoring the effect of these scanning errors in order to ascertain the limitation on maximum scanning rate in specific cases is to actually compute the beam pattern and observed the resulting distortions. The computer simulation results presented in this paper are for the sonar specifications given in fig 2.3. Using the TDI by itself, only an off-boresight sector in a quadrant can be scanned. In the computer simulation setup, a Fixed Time Wedge of opposite sense to the TDI is used to effectively deflect the on-axis sector off the boresight, which can then be scanned by the TDI. In hardware terms, this Time Wedge can be set of separate parallel CCD delay lines of incrementally varying number of delay stages, all driven with a common constant period clock (τ_f).

sonar frequency 500 KHz
unambiguous sector 30°
3 dB beamwidth 1°
line array 32 elements
element spacing d=2λ

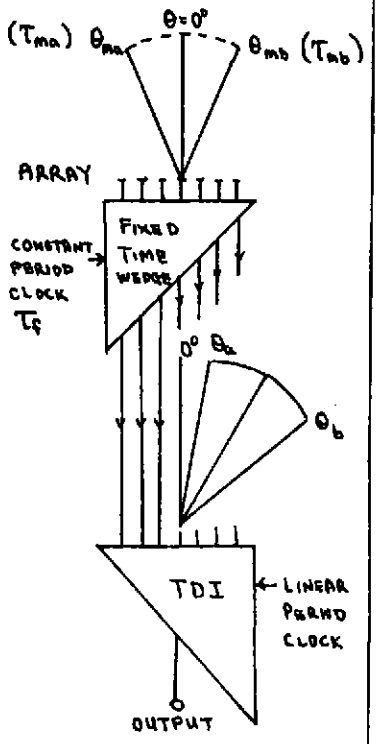

$\alpha = 2$

$\tau_{ca} = 0.2\,\mu s$ $\tau_a = 0.4\,\mu s$
$\tau_{cb} = 1.3\,\mu s$ $\tau_b = 2.6\,\mu s$
$\tau_f = 1.6\,\mu s$
$\tau_{ma} = -1.2\,\mu s$ $\theta_{ma} = -17.3°$
$\tau_{mb} = +1.0\,\mu s$ $\theta_{mb} = +14.5°$

Fig 2.3 Setup for Computer Simulation

The number of delay stages between adjacent inputs of the TDI can be defined as the 'sampling factor α' since it relates the actual clock period (which is the reciprocal of the sampling frequency) with the delay between inputs, i.e. $\tau = \alpha\tau_c$. The beam patterns Graphs G1 to G11 are computed with a sampling factor $\alpha=2$ (vertical axis 0dB to -40dB, horizontal axis -17.3° to 14.5°). The beam distortions to be observed in these plots are

(a) the reduction in magnitude of the peak response
(b) the shift in position of the peak response from the simulated target bearing
(c) the accentuated side-lobes and
(d) the non-zero nulls

From these computer simulation studies, it is concluded that, due to severe beam distortions, the maximum scanning rate for the sonar parameters of fig 2.3 is limited to around 800 Hz. It is to be noted that experimental results using a 16 input TDI device confirm this limitation. This limit does not provide sufficient range resolution for the particular sonar application. Since it is desired to scan at 8 kHz or so, an order of magnitude improvement is required. Listed out below are some of the approaches that have been attempted in trying to increase the scanning rate:-

(a) Fixed Time Compensation
(b) Subscans Approach
(c) Non-Linear Scanning
(d) Double Scanning
(e) Array Modification Approaches and
(f) Subarray Approach

Graphs G1 to G5 illustrate the deterioration in beam pattern quality as the scanning rate is increased : 500 Hz, 1 KHz, 2 KHz, 4 KHz and 8 KHz

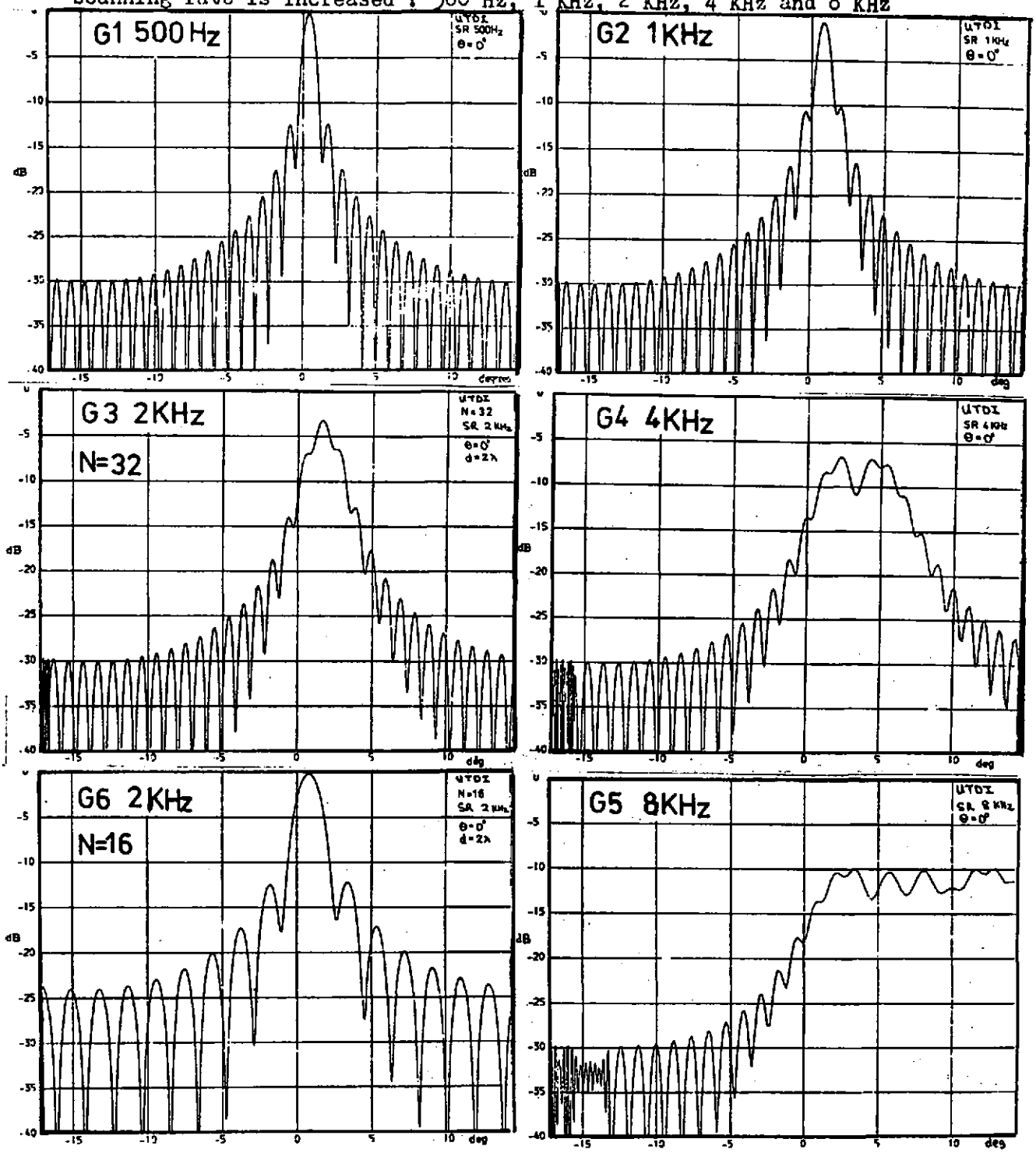

Graphs G6 and G3 show the effect of array aperture size on beam pattern quality

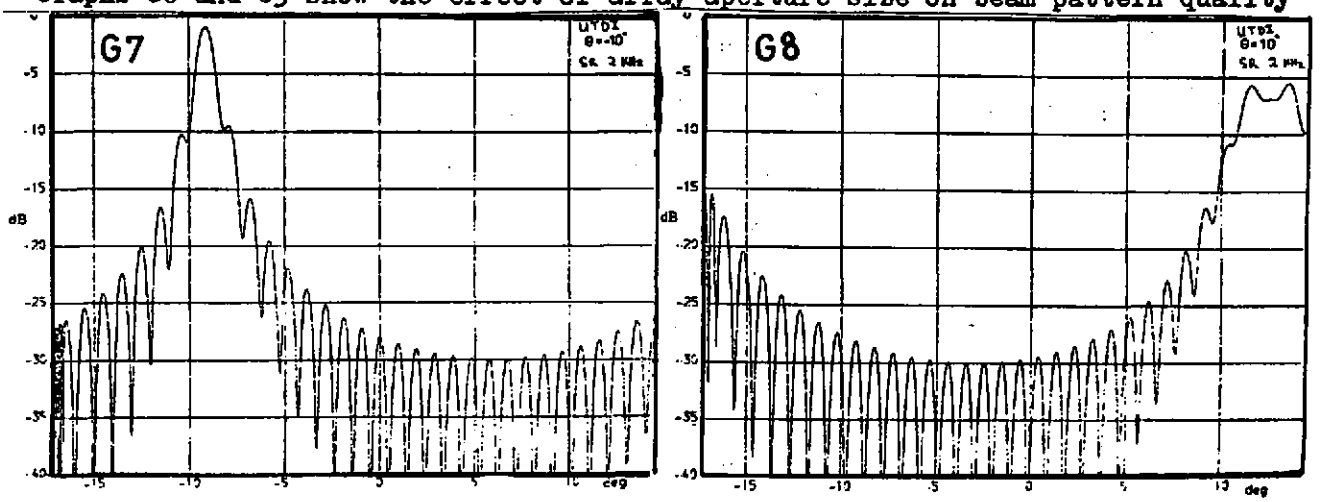

Graphs G7 and G8 demonstrate the different extents of beam distortions for different target bearings at the same scanning rate of 2 KHz

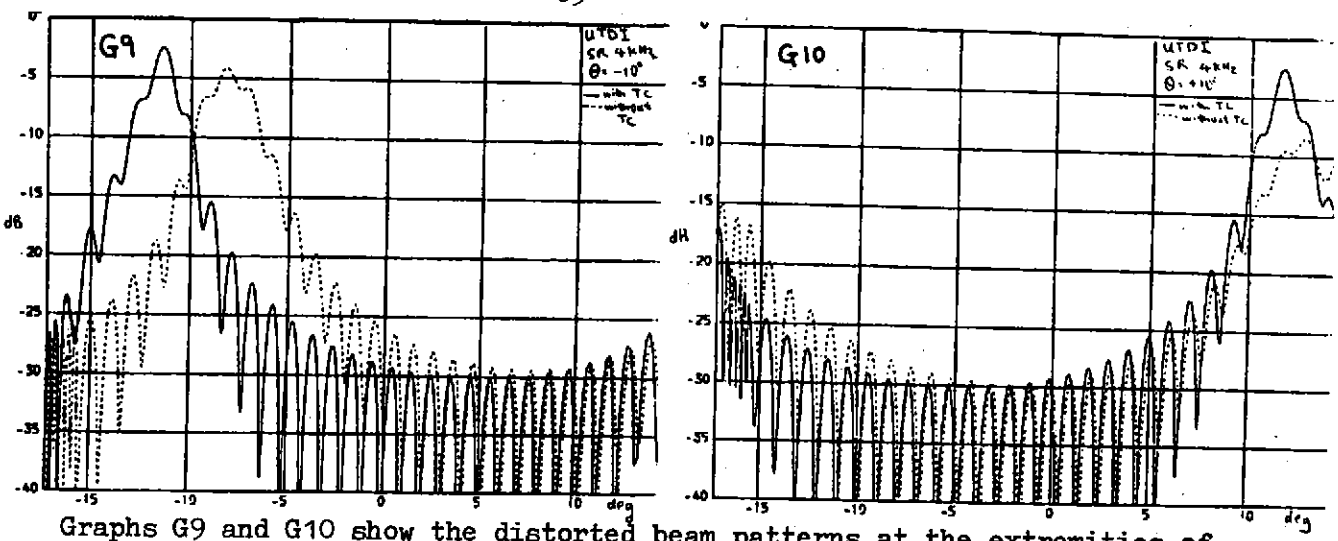

Graphs G9 and G10 show the distorted beam patterns at the extremities of the sector when the boresight direction is fixed-time compensated. The corresponding beam patterns without time compensation are shown dotted.

Because of space limitation, only fixed time compensation is briefly described here. By introducing appropriate fixed compensating time delays in the various channels before going into the TDI, the scanning time errors for ONE direction can be eliminated, thus ensuring a good beam response for that direction. However, if the boresight direction is thus compensated, the beam patterns for the extremities of the sector remain unduly distorted. It is to be noted that Graphs G9 and G10 are obtained using EXACT theoretically calculated compensating time dealys which in practice may not be easy to realise exactly. This and the other approaches do not provide the required improvement in the scanning rate.

III Novel Device Concept for High Speed Scanning

Fig 3.1 shows plane waves impinging on a line array of equally spaced transducers connected to the new device for which the number of delay stages X_n from each input to the output is as yet unkown. It has already been mentioned that linear period scanning clock operation is desirable, but more significantly, it can be shown to be a necessary condition for the evolution of a scanning device structure with common clocking. Consider an instant t_p in the scan when the instantaneous clock period is τ_{cp}. At this instant, the device output is to represent a plane wavefront incident at an angle Θ_p. To ensure that the past input samples constituting this particular output sample all come from the particular wavefront, the number of delay stages must be such that the cummulative delay over the past X_n consecutive clock periods for each input is equal to the relevant delay in water, i.e. for the particular Θ_p and τ_{cp},

(electronic time delay CD over X_n stages)=(water delay AB) for all n

For a general scanning law, the value of X_n to satisfy this condition for each n will in general be different for different values of τ_{cp} and Θ_p so that a particular device structure can be configured for the particular value of Θ_p, but will be invalid for all other angles. However, for a linear scanning law, it is shown that X_n is indeed independent of Θ_p and τ_{cp}. Appendix I shows that the linear period law results in the successive clock periods forming a geometrical progression with a common ratio γ. Therefore, for the n th input,

$$\frac{\tau_{cp}}{\gamma^{X_n} - 1} \left\{ \frac{\gamma^{X_n} - 1}{\gamma - 1} \right\} = (n - 1)\alpha\tau_{cp}$$

Solving for X_n, $X_n = \log[\gamma/(\gamma - r^{n-1}\alpha)] / \log(\gamma)$

That X_n is independent of the actual value of the instantaneous clock period τ_{cp} with which the analysis begins, is of crucial significance because it means that the same values of X_n are valid for ALL values of τ_{cp} and θ_p, and hence throughout the scan. The quality of the beam pattern should therefore be the same over the hole sector. This is to be con trasted with the deteriorating beam quality towards one edge of the sector in the case of the existing device. X_n depends only on the rate of change of clock period r. Using the sonar parameters in fig 2.3 and for a scanning rate of 8 kHz, the value of r is 0.0088. With this value of r and α=2, the calculated values of X_n are tabulated in fig 3.2, which are in general not integers. Since in any hardware realization of a practical device, only integral numbers of delay stages are possible, X_n can only be approximated. Fig 3.2 also shows X_n corrected to the nearest integer. The histograms of X_n against n for the new device and the existing device have been plotted for comparison. Clearly, the fundamental difference is that with the new device, X_n is a non-linear function of n so that the number of delay stages between adjacent inputs depends on the positions of the respective inputs whereas in the existing device, all the adjacent inputs are separated by the same number of delay stages. Because of this non-uniform structure, the new device will henceforth be called the NUTDI[2](for Non-Uniform TDI) to distinguish it from the UTDI (Uniform TDI).

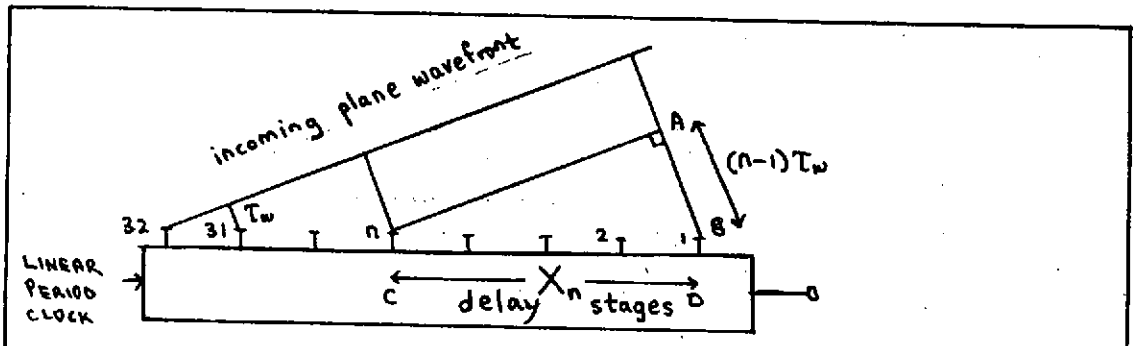

Fig 3.1 Towards a new device structure

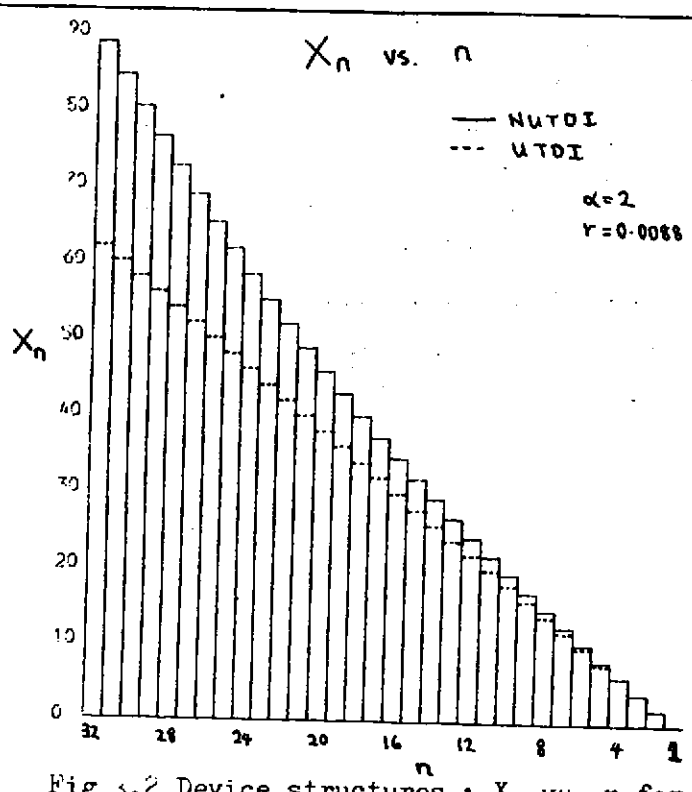

	NUTDI	UTDI
XI	INTEGER	
68.836	69	62
64.582	65	60
60.479	60	58
76.516	77	56
72.690	73	54
68.966	69	52
65.396	65	50
61.920	62	48
58.545	59	46
55.267	55	44
52.060	52	42
48.960	49	40
45.962	46	36
43.021	43	36
40.155	40	34
37.356	37	32
34.629	35	30
31.963	32	26
29.358	29	26
26.812	27	24
24.320	24	22
21.862	22	20
19.496	19	18
17.157	17	16
14.866	15	14
12.620	13	12
10.418	10	10
8.257	8	8
6.136	6	6
4.054	4	4
2.009	2	2
0.000	0	0

Fig 3.2 Device structures : X_n vs. n for NUTDI and UTDI

All the NUTDI beam patterns on this page are at 8 KHz scanning rate

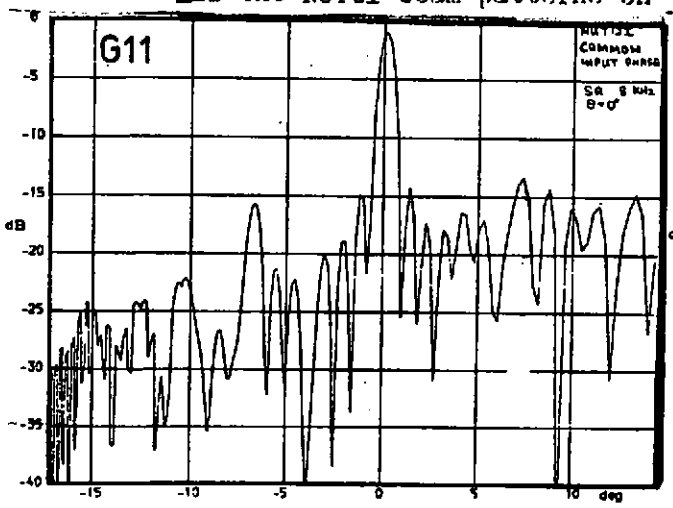

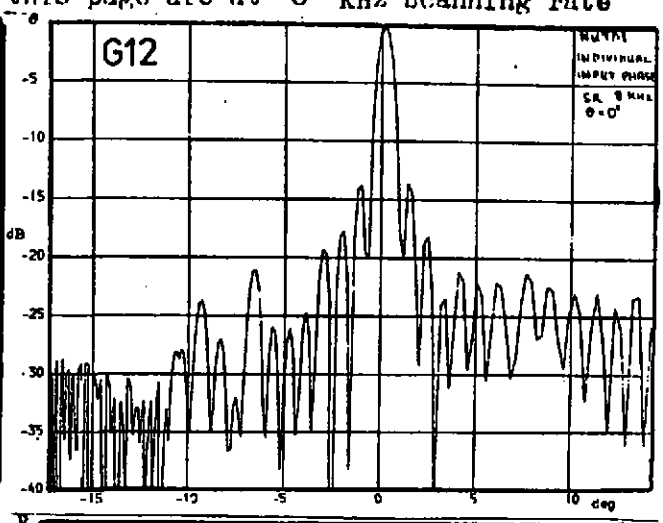

Graph G11 : Common input phase
Graph G12 : Individual input phase
Graph G13 : Fixed phase compensation $\theta=0^\circ$

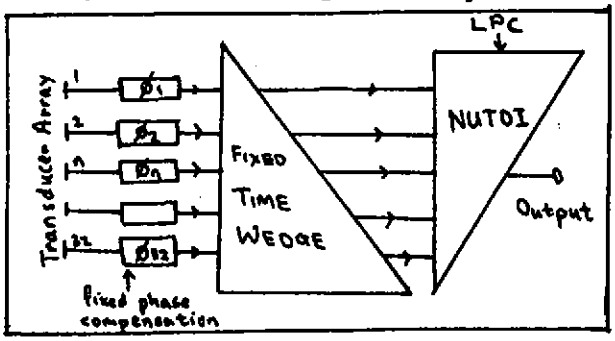

Fig 3.6 Fixed phase compensation $\theta=0^\circ$

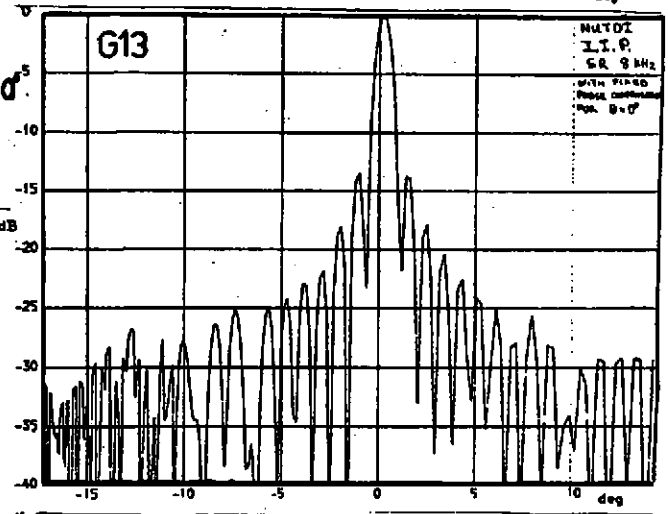

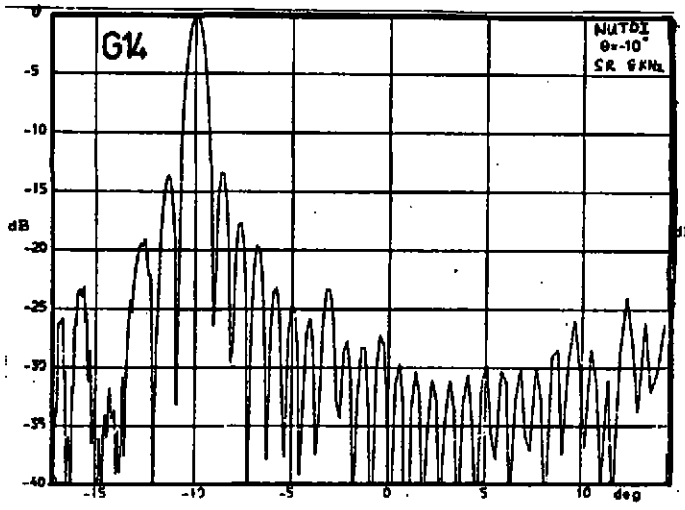

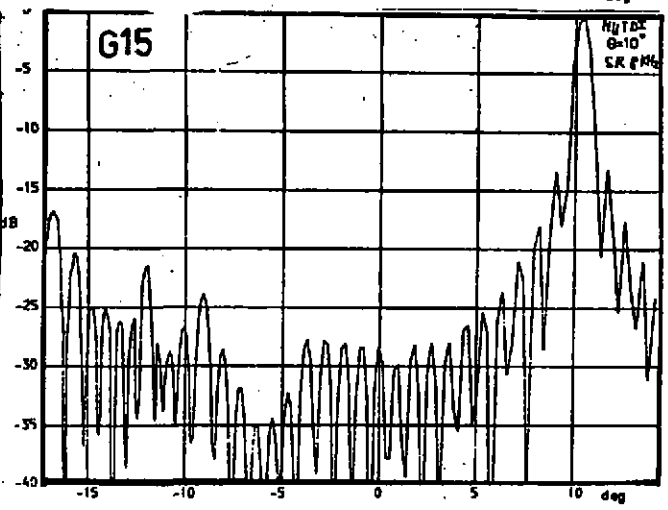

Graphs G13, G14 and G15 demonstrate the uniform beam quality for different target bearings (to be contrasted with G3, G7 and G8 for the UTDI)

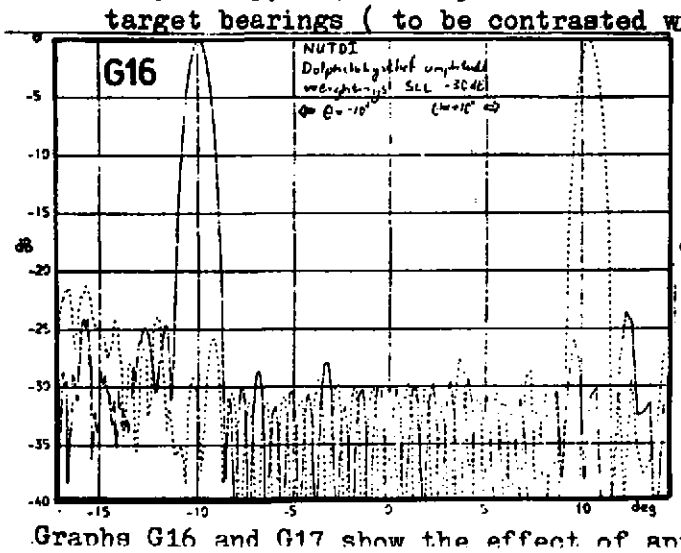

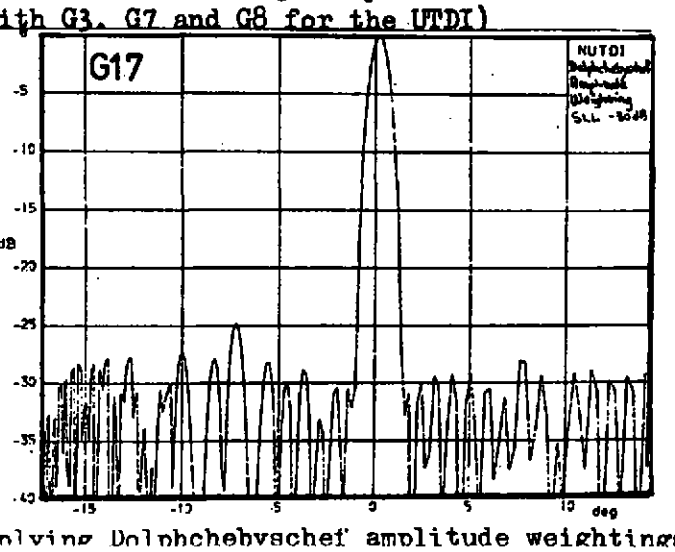

Graphs G16 and G17 show the effect of applying Dolphchebyschef amplitude weightings

Graph G11 shows the beam pattern obtained using the NUTDI structure at 8 kHz scanning rate. Though much better than that obtained with the UTDI (of Graph G5), it is still far from perfect and in particular, the far-out side-lobes are high especially in that part of the sector corresponding to large clock periods. The imperfections are due to what will be called 'quantisation time errors' (QTE) incurred when X_n are approximated to the nearest integers. Though these QTE are fixed fractions of the clock periods, their absolute magnitudes increase with larger clock periods, thus giving rise to the distortions in the corresponding part of the sector. In theory, the QTE can be reduced by using device structures based on larger values of the sampling factor α. This is because, to achieve the same differential delays, a larger α means smaller clock periods and hence smaller QTE. However, difficulties encountered in high frequency operation of a practical device (e.g. charge transfer efficiency deterioration and variation with clock frequency) as well as peripheral circuitry considerations limit the maximum realistic value of α to 2, which is the value used in the simulation.

However, the present TDI input scheme can be modified to reduce the QTE without requiring a larger value of α and thus without necessitating any further increase in the high clock frequency of the device. For a three phase CCD, three phase clocking (fig 3.3) is necessary to ensure an unidirectional transfer of charge. A set of three adjacent electrodes constitutes a 'delay stage'. Presently, all the inputs are sampled simultaneously on a common phase (e.g. phase 1 in fig 3.4) so that the differential delay between adjacent inputs can only be an integral number of phase clock periods. However, differential delays which include fractions (1/3 or 2/3) of a phase clock period can be effected by clocking each input on an appropriately chosen phase. In device structure terms, this involves introducing one or two additional electrodes at the appropriate inputs as shown in fig 3.5. Graph G12 shows the improvement in beam quality resulting from this modification, which effectively allows the values of X_n to be approximated to the nearest one-third instead of to the nearest integer and thereby reducing the QTE by a factor of 3. The delay quantum is now the master clock period instead of the phase clock period.

Even with this modification, the beam pattern is still not ideal because there remain QTE which are within $\pm$ 1/6 of the clock period. The remaining QTE for one direction can be eliminated by introducing residual fixed phase compensation in the various channels (fig 3.6). Graph G13 shows the improvement in beam quality when the boresight direction is thus compensated. It is to be noted that the phase compensation required are so small that they do not adversely affect the beam quality for target bearings at the extremities of the sector (Graphs G14 and G15). The uniform good quality of the beam pattern for all target bearings is a crucial advantage the NUTDI has over the UTDI.

The computer plots so far referred to are with uniform amplitude weighting. Graphs G16 and G17 show the effect of applying Dolphchebyschef amplitude weightings calculated for a side-lobe level of -30 dB.

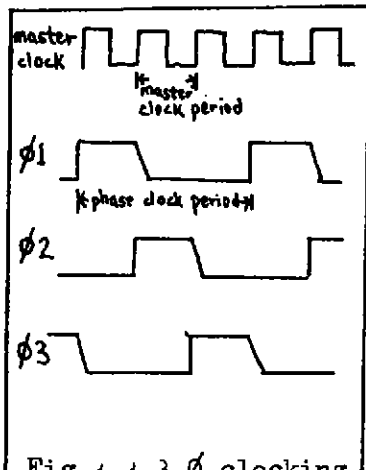

Fig 3.3 3 ϕ clocking

X_n	INTEGER	INPUT PHASE
31.96	32	ϕ1
29.35	29	ϕ1
26.81	27	ϕ1
24.32	24	ϕ1
21.88	22	ϕ1

Fig 3.4 common input phase

X_n	INT.	FRACTION	INPUT PHASE
31.96	32	0	ϕ1
29.35	29	1/3	ϕ3
26.81	26	2/3	ϕ2
24.32	24	1/3	ϕ3
21.88	22	0	ϕ1

Fig 3.5 individual input phase

An inherent feature of time delay beam scanning is the existence of a 'cross-over' time at the beginning of a scan. During this 'cross-over' time, the output samples are not fully constituted from valid inputs but are partly corrupted with inputs which are 'cross-overs' from the previous scan. The magnitude of the 'cross-over' time is equal to the initial cummulative time that the first sample from the first input takes to traverse the whole length of the device before emerging at the output as a constituent of the first fully valid output sample in the present scan. It is to minimize this 'cross-over' time that the linear period clock is swept from small to large periods. The 'cross-over' time can be observed on the computer plots.

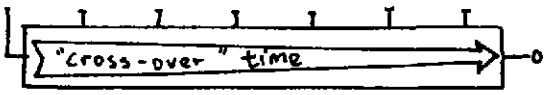

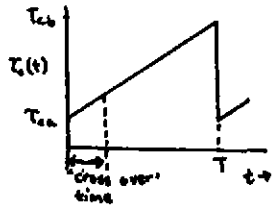

IV. Conclusion

It has been demonstrated that for within-pulse sector scanning, existing TDI devices produce beam distortions which depend on sector size, beamwidth and scanning rate. For the particular case of a 500 kHz sonar with a 1 degree beam swept over a 30 degree sector, the maximum scanning rate has been ascertained to be 800 Hz, at which the range resolution is not sufficient. A new device (NUTDI) is described and shown to be capable of scanning at 8 kHz for the afore-mentioned sonar application without severe beam distortions. It is to be noted that this new device is only a particular embodiment of a more general device concept which is applicable not only to sonar but also to time delay beam scanning in general. The new device is currently in the fabrication stage and experimental work is proceeding for its incorporation in a prototype scanning sonar system. Future extension of this work to two dimensional scanning using either an orthogonal Tx/Rx cross array or a full N X N matrix array is envisaged. The system simplicity and compactness resulting from the use of both TDI and NUTDI devices for the latter system may be over-riding considerations when compared with other approaches.

References

1. Vanstone, G. F., Harp, J. G., Roberts, J.B.G. : 'A Time Delay and Integration CCD for Serial Scannned IR Imagers', Int.Conf.Applications of CCDs, Edinburgh, 1976

2. Ong, L. H., : Patent Application Nos. 41849/78 and 44568/78

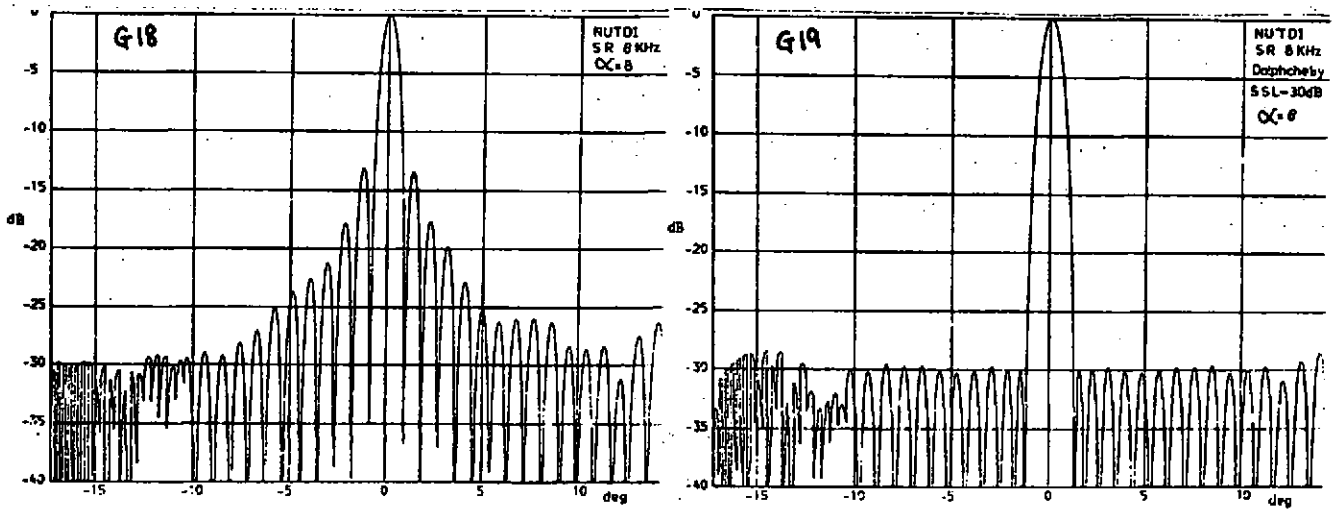

Graphs G18 and G19 show the beam patterns obtained using a device structure with a sampling factor α of 8 for uniform and Dolphchebyschef amplitude weightings respectively.

Acknowledgements

Thanks are due to G. Harp of R.S.R.E for device fabrication and to Professor E.D.R.Shearman, Dr.H.O.Berktay*, Dr.P.N.Denbigh and Dr.D.C.Cooper of the University of Birmingham and to Dr.J.B.G.Roberts and Dr.D.V.McCaughan of R.S.R.E. for their encouragement in this work.

* Now with the University of Bath, U.K.

Appendix I

Let the TDI clock period be swept linearly from a minimum value τ_a to a maximum value τ_b in a time interval T . The rate of change r of clock period is

$$r = \frac{d\tau}{dt} = \frac{\tau_b - \tau_a}{T}$$

Let $\gamma = 1 + r$.

If t_k represents sampling instants in a scan, then

at the beginning of scan, $t_o = 0$

After the first delay $\tau_1 = \tau_a$

the next sampling instant $t_1 = \tau_a$

next incremental delay $\tau_2 = \tau_a + r\tau_a = \tau_a\gamma$

$\therefore$ next sampling instant $t_2 = t_1 + \tau_2 = \tau_a + \tau_a\gamma$

next delay $\tau_3 = \tau_2 + r\tau_2 = \tau_2\gamma = \tau_a\gamma^2$

$\therefore$ next sampling instant $t_3 = t_2 + \tau_3$

$= \tau_a + \tau_a\gamma + \tau_a\gamma^2$

- - - -

- - - -

By induction,

the k^{th} delay $\tau_k = \tau_a\gamma^{k-1}$

and the k^{th} sampling instant $t_k = \tau_a \frac{(\gamma^k - 1)}{(\gamma - 1)} = \frac{\tau_a}{r}(\gamma^k - 1)$

At the end of a scan, $t_{ke} = T$

i.e. $\frac{\tau_a}{r}(\gamma^{ke} - 1) = T = \frac{\tau_b - \tau_a}{r} = \frac{\tau_a}{r}\frac{\tau_b}{\tau_a} - 1$

Solving for k_e,

$$k_e = \frac{\log\left(\frac{\tau_b}{\tau_a}\right)}{\log(\gamma)}$$

$\therefore$ within a scan, k goes from 1, 2... to k_e' where k_e' is the largest integer less than k_e.